

# Multi-Disease Classification of 13,667 Body CT Scans Using Weakly Supervised Deep Learning

Original Research

Fakrul Islam Tushar<sup>a,b</sup>, Vincent M. D'Anniballe<sup>a</sup>, Rui Hou<sup>a,c</sup>, Maciej A. Mazurowski<sup>a,c</sup>, Wanyi Fu<sup>a,c</sup>, Ehsan Samei<sup>a,c</sup>, Geoffrey D. Rubin<sup>d</sup>, Joseph Y. Lo<sup>a,c</sup>.

<sup>a</sup>Department of Radiology, Duke University, Durham, NC 27705 USA.

<sup>b</sup>Erasmus+ Joint Master in Medical Imaging and Applications, University of Girona, Girona, Spain.

<sup>c</sup>Department of Electrical and Computer Engineering, Duke University, Durham, NC 27705 USA.

<sup>d</sup>Department of Medical Imaging, University of Arizona, Tucson AZ.

## Summary:

A rule-based algorithm enabled automatic extraction of disease labels from tens of thousands of radiology reports.

These weak labels were used to create deep learning models to classify multiple diseases for three different organ systems in body CT.

## Key points:

- Labels extracted by the rule-based algorithm were 91 to 99% accurate by manual validation.
- Deep learning models developed for each of three organs systems (lungs/pleura, liver/gallbladder, and kidneys/ureters) enabled the classification of multiple diseases with AUCs ranging from 0.65 to 0.97, 0.62 to 0.89, and 0.68 to 0.92, respectively.
- Given these promising initial results, weak labeling may leverage vast amounts of existing report and image data to create deep learning models to classify multiple diseases in multiple organ systems.

### Background

Training deep learning classifiers typically requires massive amounts of manual annotation. Weak supervision may leverage existing medical data to classify multiple diseases and organ systems.

### Purpose

To design multi-disease classifiers for body computed tomography (CT) scans using automatically extracted labels from radiology text reports.

### Materials & Methods

This retrospective study deployed rule-based algorithms to extract 19,255 disease labels from reports of 13,667 body CT scans of 12,092 subjects for training. Using a 3D DenseVNet, three organ systems were segmented: lungs/pleura, liver/gallbladder, and kidneys/ureters. For each organ, a 3D convolutional neural network classified normality versus four common diseases. Testing was performed on an additional 2,158 CT volumes relative to 2,875 manually derived reference labels.

### Results

Manual validation of the extracted labels confirmed 91 to 99% accuracy. Performance using the receiver operating characteristic area under the curve (AUC) for lungs/pleura labels were as follows: atelectasis 0.77 (95% CI: 0.74 to 0.81), nodule 0.65 (0.61 to 0.69), emphysema 0.89 (0.86 to 0.92), effusion 0.97 (0.96 to 0.98), and normal 0.89 (0.87 to 0.91). For liver/gallbladder: stone 0.62 (0.56 to 0.67), lesion 0.73 (0.69 to 0.77), dilation 0.87 (0.84 to 0.90), fatty 0.89 (0.86 to 0.92), and normal 0.82 (0.78 to 0.85). For kidneys/ureters: stone 0.83 (0.79 to 0.87), atrophy 0.92 (0.89 to 0.94), lesion 0.68 (0.64 to 0.72), cyst 0.70 (0.66 to 0.73), and normal 0.79 (0.75 to 0.83).

### Conclusion

Weakly supervised deep learning classifiers leveraged massive amounts of unannotated body CT data to classify multiple organ systems and diverse diseases.

## I. INTRODUCTION

Artificial intelligence (AI) has the potential to revolutionize disease diagnosis, exemplified by the widespread application of machine learning algorithms for classification, segmentation, and detection tasks (1-4). Despite the potential, most disease classification AI algorithms target only a single organ or disease making their scope significantly narrower than that of clinical practice (5, 6). Currently, the major bottleneck for developing multi-disease AI algorithms is a lack of annotated data. Training these algorithms has traditionally relied on manually labeling large numbers of medical images, requiring rigorous standardization, clinical expertise, and significant time commitment (7). The hand labeling of abnormalities is challenging even for single radiographs but becomes even more impractical for the many images associated with a single cross-sectional imaging study acquired with computed tomography (CT).

Ample training data already exist in the electronic health record. Unlike supervised learning, which relies on well-annotated data, weakly-supervised learning allows the use of incomplete or inaccurate data. Although less precise than hand labeling, weak supervision enables the systematic processing of vast amounts of disease information from existing radiology text reports by automatically labeling medical images thereby mitigating the need for human annotation. This approach has already yielded several large medical imaging datasets (8-10). For CT specifically, DeepLesion is a dataset developed from the report text of almost 11,000 CT studies with over 32,000 lesions identified in multiple organs (11-14). In other studies using report text for weak labeling, Draelos *et al.* (15) annotated up to 83 thoracic abnormalities in over 36,000 chest CT volumes, and Eyuboglu *et al.* (16) annotated up to 96 anatomical regions in over 6,000 whole body FDG-PET/CT exams. These studies demonstrate the feasibility of weakly supervised annotation of large datasets to enable deep learning in medical imaging.

In this study, we employ weak supervision to provide multi-disease classification of body CTs of the chest, abdomen, and pelvis based on existing radiology reports. Body CTs were selected because they are performed commonly and encompass a variety of organs and diseases within a large portion of the body. A rule-based algorithm (RBA) was chosen to extract disease labels because it can achieve high accuracy and is readily adjustable to tackle new or expanded tasks. We focused on three organ systems: lungs/pleura, liver/gallbladder, and kidneys/ureters; these were chosen because they represent large structures with very different anatomical

appearance, location, and range of disease manifestations. We hypothesized that a weak supervision framework based on radiology report text would allow a CNN model to classify multiple diseases, even without information about the disease location, and despite the heterogeneous appearance of each organ/disease.

## II. MATERIALS AND METHODS

Institutional Review Board approval was obtained, and informed consent was waived for this retrospective study that was compliant with the Health Insurance Portability and Accountability Act. Our earlier work in CT disease classification was trained on much smaller subsets of fewer than 1,600 cases to classify a single disease of the chest (17). A related study performed classification of multiple chest diseases, but was limited to non-contrast chest CTs (15). Compared to our previous study on automated labeling (18, 19), we have refined the rule-based algorithms and increased the number of cases as well. The current study represents our most diverse effort, where we have demonstrated the multi-label classification of diseases while expanding to three different organ systems (lungs/pleura, liver/gallbladder, and kidneys/ureters) in chest, abdomen, and pelvis CTs.

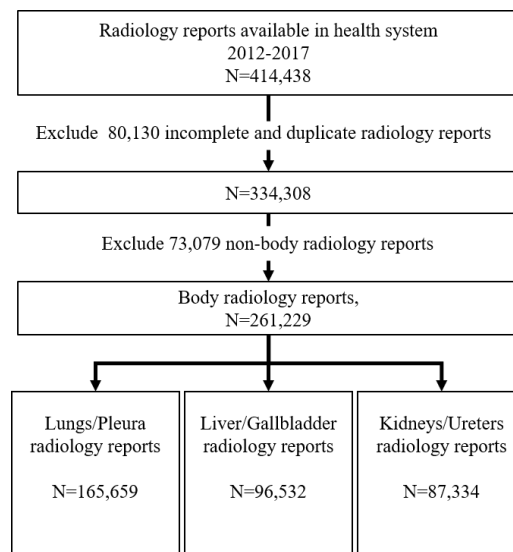


**Figure 1.** Flowchart shows cohort selection. From 414,438 radiology reports performed between 2012 to 2017, a set of 261,229 body radiology reports was selected after excluding incomplete, duplicate and non-body reports.

N=number of reports. Note that the sum of reports for each organ system does not correspond to the total number of body radiology reports, because a single subject could have multiple findings across multiple organ systems.

#### *A. Disease label and Dataset Mining*

Labels were extracted from the free-text radiology reports using a rule-based algorithm (RBA) to label body CT studies performed between 2012 and 2017 (20). The algorithm is described in the code repository (<https://gitlab.oit.duke.edu/railabs/LoGroup/multi-label-weakly-supervised-classification-of-body-ct>) Among these studies, 165,659 reports were used to extract labels from the lungs/pleura, 96,532 reports for liver/gallbladder, and 87,334 reports for kidneys/ureters shown in Figure 1, where one report could have multiple diseases in one or more of these organ systems. Only the findings section of the report was used to limit labels to image-based information and to minimize the influence of other factors such as scan indication or previous medical history. The findings section was tokenized into sentences and processed in series by a set of rules.

The rules were built upon general relationships, which can be applied to different organs by adding keywords to the dictionary. For example, *if* a sentence contained the organ name “liver” or “hepatic” *and* abnormality “lesion,” *and* without any negation keywords like “no” or “without,” *then* the label was positive for liver lesion. By substituting other organ names such as “kidney” or “renal,” the same rule would apply to kidney lesions. By using approximately 30 rules and 500 keywords, this method could be applied to different organs and diseases, such as renal atrophy or pleural effusion.

The labels were considered “weak” for two reasons: 1) they were applied to the entire volume without disease localization, and 2) the rule-based decisions included some expected imperfections due to its automated implementation on existing report data. To estimate the actual accuracy, the reference standard for labeling was established for a randomly selected test set of 2,158 reports, which were manually assigned disease labels by a graduate student with gross anatomy training (V.M.D.) supervised by a board-certified radiologist (G.D.R.). The rationale for this reference standard was that a smaller representative subset of manually labeled reports was

practicable, whereas labeling all 165,659 reports would have been prohibitive in both cost and time.

This dataset represents a typical clinical cohort, in which subjects may undergo multiple scans or have multiple positive findings. Furthermore, this cohort encompassed CT exams from a large health system that was not limited to any acquisition, or reconstruction type. The CT manufacturers were Siemens and GE. The RBA identified 19,255 case-level labels in 13,667 CT volumes from 12,092 subjects. The lungs/pleura were labeled as normal versus having one or more of four diseases: atelectasis, nodule, emphysema and/or effusion. The liver/gallbladder were labeled as normal or stone, lesion, dilation, and/or fatty. The kidneys/ureters were labeled as normal or stone, lesion, atrophy, and/or cyst. These abnormalities were selected based on their high prevalence and varied appearance. Each abnormality or “disease” may comprise multiple keywords that were grouped together based on similarity of language or overlap in image appearance. For example, lung nodule and mass were grouped into the nodule class; biliary calculus, calcification, and gallstone to liver stone class; and fatty liver and steatosis to fatty liver class. The RBA labeled a report as “normal” only in the absence of dozens of other diseases that were not otherwise analyzed in this study.

## **B. *Image Segmentation***

A segmentation model was used to guide extraction of organ-specific patches from CT volumes for subsequent classification. [Figure 2](#) shows the overall classification pipeline used in this study. The DenseVNet (21) segmentation model was trained with the 4D extended cardiac-torso (XCAT) dataset (22), which contains CT volumes and corresponding multi-organ segmentation masks. The 50 XCAT volumes were randomly assigned into 44 training and 6 validation. Because the XCAT training set contains normal anatomy only, segmentation errors were observed when the normally aerated lungs were replaced by disease. The segmentation model was fine-tuned using 30 additional, randomly selected, diseased lung cases (10 edema, 10 atelectasis, 7 pneumonia, and 3 nodule). The resulting segmentation masks were then manually corrected to the lung margins. These 30 diseased cases with corrected segmentation were combined with 10 normal XCAT training cases and used to fine-tune and produce the final segmentation model. The initial segmentation model performed well on both normal and diseased liver and kidneys cases, so no further fine-tuning of the segmentation model was performed for those two organs. Organ masks were

not available for the gallbladder and ureters, so those were included within expanded patches that contained the liver and kidneys respectively as described in the next section.

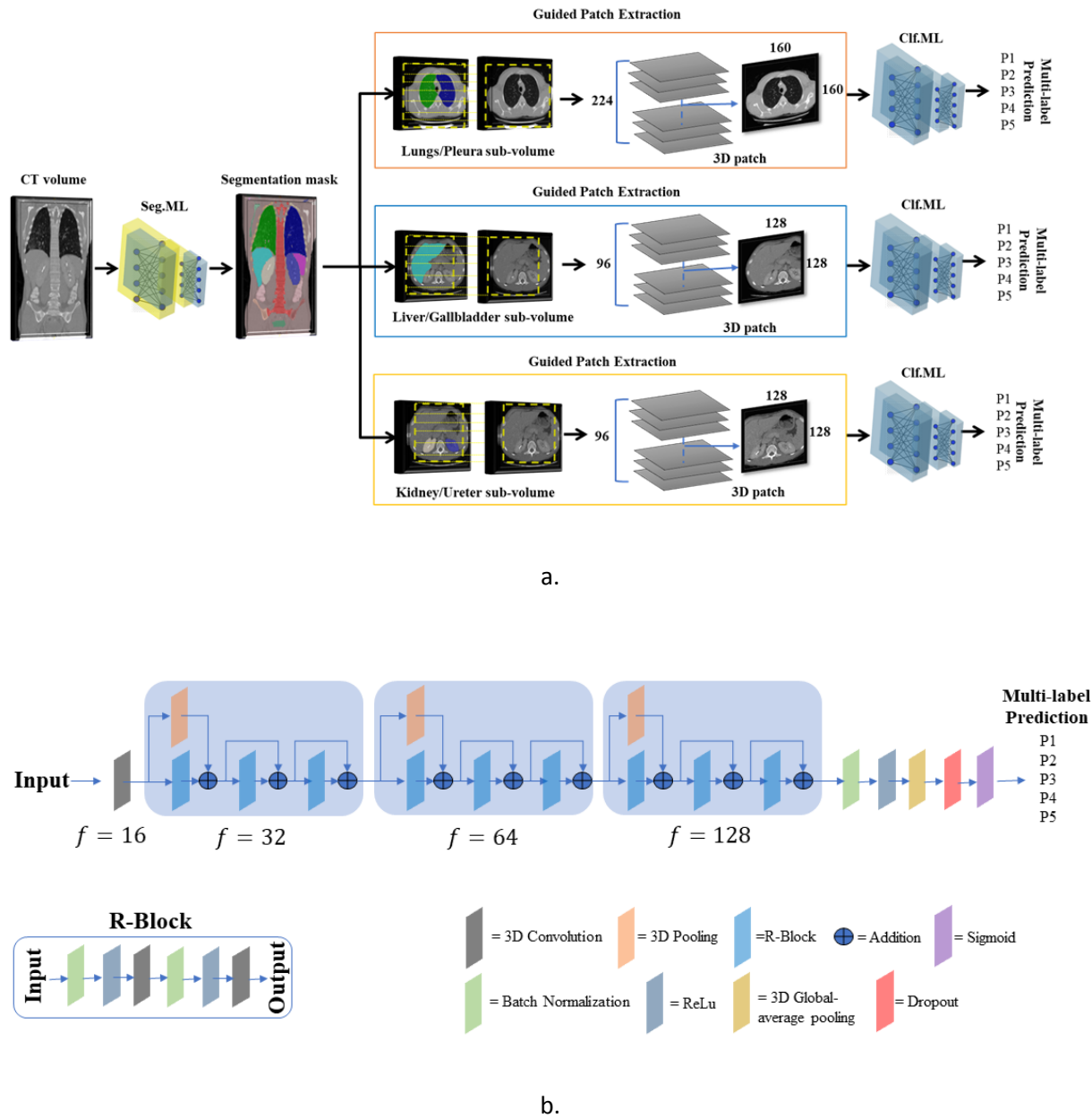


**Figure 2.** Overall classification framework and functional architectures. (a) The Classification framework includes two networks denoted as Seg.ML=segmentation module and Clf.ML=classification module. The segmentation module is a DenseVNet (21) network, producing major organ masks such as lungs, liver, and kidneys. Expanded 3D patches were extracted, which were centered/offset for each organ based on the segmentation masks. Finally,

extracted 3D patches were fed to the classification module for the final classification score. (b) The classification module is a 3D Resnet-like model with 3 R-Blocks in each resolution. Number of filters is denoted as  $f$ . Final output is a tensor of probabilities for desired multiple labels (diseases).

### C. *Pre-processing and Weakly Supervised Image Classification*

Prior to classification, all CT volumes were resampled to voxels of size  $2\text{ mm} \times 2\text{ mm} \times 2\text{ mm}$  via B-spline interpolations, clipped to intensity range (-1000, 800) HU for lungs/pleura, (-200, 500) HU for liver/gallbladder and kidneys/ureters, and normalized to 0 mean and 1 standard-deviation. To reduce computational expense and the influence of background organs, 3D patches were placed around each organ:  $224 \times 160 \times 160$  (Z×W×H) for lungs/pleura and  $96 \times 128 \times 128$  (Z×W×H) for both liver/gallbladder and kidneys/ureters. Patch sizes were based on organ size plus a margin to allow for patient variability and to include most or all of the gallbladder in the liver/gallbladder and ureters in the kidneys/ureters systems. The segmentation module was used to guide individualized placement of patches, and kidney patches were offset anteriorly to remain within the body. For each organ, the CT volumes were randomly divided into subsets to train (70%), validate (15%), and test (15%) the model. Splitting was performed by subject and separately for normal vs. diseased classes per organ system to preserve disease prevalence across each subset.

The architecture of the 3D CNN used in this study was inspired by Resnet (23). As shown in [Figure 2b](#), features were learned in three resolution scales. After each resolution, the features were halved by max-pooling, and the number of filters was doubled. After the 3rd resolution, the last R-block features were passed through batch-normalization, ReLu, global max-pooling, dropout, and finally sigmoid classification layer for the multi-label predictions. Adam was used to optimize the weights, and weighted cross-entropy was used as the loss function. The uniform distribution did initialization of the weights. In order to retain the natural prevalence and cooccurrence of diseases, no class-balancing was performed during training.

Training took approximately 26 hours for segmentation (Python TensorFlow v1.5) and 40 hours for classification (Python TensorFlow v2.0) using 4 TITAN RTX GPUs (Nvidia Corporation, Santa Clara, CA). All models' weights, initial



hyper-parameters, and code are publicly available (<https://gitlab.oit.duke.edu/railabs/LoGroup/multi-label-weakly-supervised-classification-of-body-ct>). The 13,667 CT volumes and labels will also become publicly available pending institutional approval.

#### *D. Statistical Analysis*

Performance was assessed using the receiver operating characteristic (ROC) area under the curve (AUC). 95% confidence interval (CI) was calculated by using package pROC 1.16.2 in R 3.6.1 with 2000 iterations of bootstrapping (24).

### III. RESULTS

#### *A. Study Sample Characteristics and Demographics*

Case-level labels for this study were generated by the RBA for 19,255 findings in 13,667 CT volumes from 12,092 subjects. [Figure 3](#) shows the total dataset and distribution of labels, volumes, and unique subjects among the three targeted organs.

The study population was from a health system composed of multiple hospitals. The average age of the subjects was  $57 \pm 18$  years; the median age was 61 years. The overall percentage of women was 51% (6,172 of 12,092 subjects). Among the 13,667 CT volumes, 72% (9,836 of 13,667) were with contrast and 28% (3,831 of 13,667) were without contrast. The 13,667 CT volumes consisted of 5 protocols: 5,099 (37%) chest-abdomen-pelvis, 5,085 (37%) abdomen-pelvis, 2,886 (21%) chest, 488 (4%) abdomen, and 109 (1%) chest-abdomen. We did not perform any exclusion based on age, scanner equipment/protocols, contrast, or type of reconstruction.

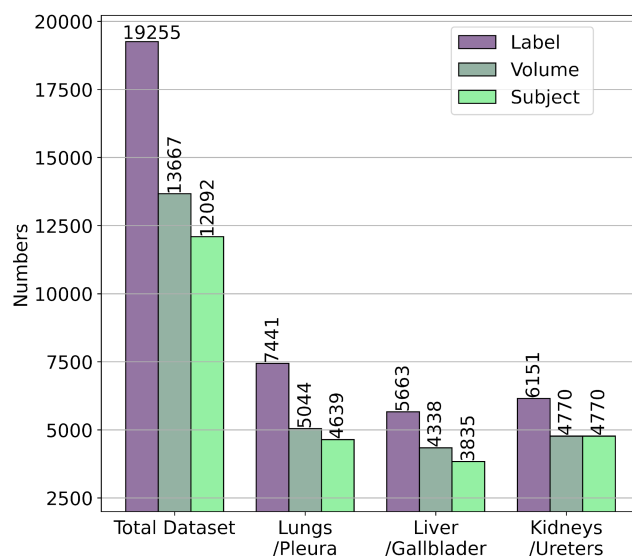
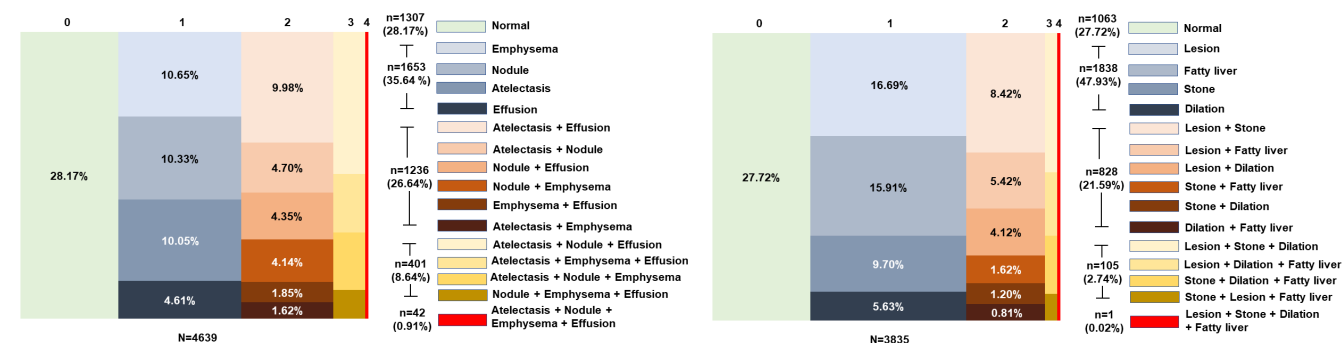


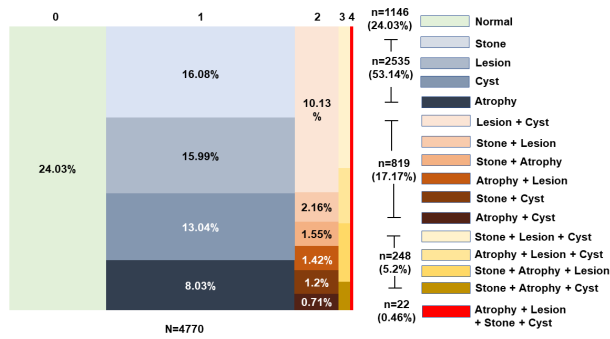
**Figure 3.** Distribution among 3 organ systems of 19,255 case-level labels from 13,667 CT volumes of 12,092 unique subjects.

**Table 1** shows the number of volumes used in classification tasks for each organ system. For each of the three organ systems, the RBA labeled each case as normal versus having one or more of four diseases. **Figure 4** illustrates the co-occurrence and association between diseases for this multi-label data set. The test subset consisted of 2,158 (lungs/pleura=771, liver/gallbladder=652, kidneys/ureters=749) CT volumes from 2,133 unique subjects with 1,154 labels for lungs/pleura, 787 labels for liver/gallbladder and 934 labels for kidneys/ureters.



a.

b.



C.

Figure 4. a-c for the lungs/pleura, liver/gallbladder, and kidneys/ureters (respectively), tree maps show occurrence and co-occurrence of targeted diseases among unique subjects. Column headers 0, 1, 2, 3 and 4 represent the number of abnormalities within a subject. Area of any column or cell corresponds to frequency for those combination(s) of diseases. For example, in Fig. 4a, column “1” atelectasis (10.05%) and column “2” atelectasis + effusion (9.98%) have the same area. N= number of unique subjects per organ system, n= number of unique subjects belonging to that (co-)occurrence. Percentage of n/N is noted.

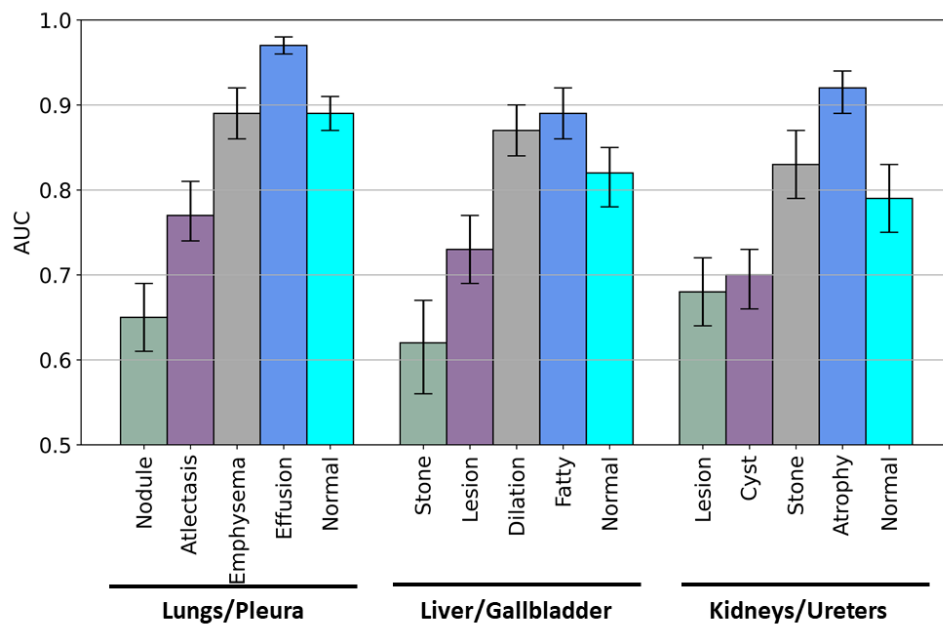
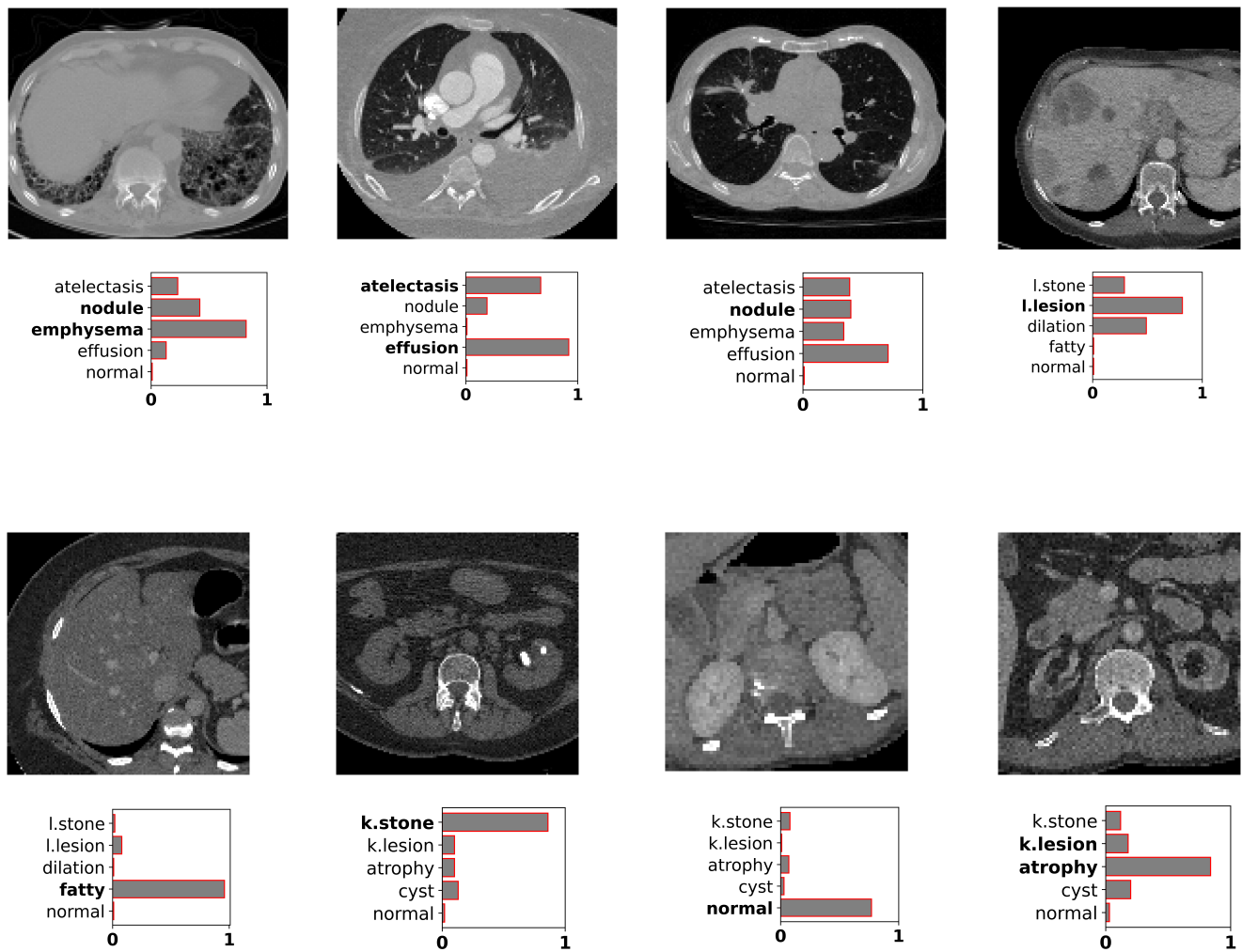


Figure 5. Test ROC AUCs for multi-label classification of CNNs for (left to right) lungs/pleura, liver/gallbladder, and kidneys/ureters. Error bars represent 95% confidence intervals .

Label noise is an expected consequence of large and diverse medical imaging datasets. When compared to manually validated labels, the 2,875 RBA-derived labels in the test set were identified with accuracy from 91% to 99%, and F-score from 0.85 to 0.98. [Table 2](#) displays the labeling accuracy for each organ system and disease class.

[Figure 5](#) shows the performance of the multi-label classification models for the lungs/pleura, liver/gallbladder, and kidneys/ureters, with ground truth based on the manually obtained test set labels.



[Figure 6](#). Multi-label multi-organ models predictions relative to ground truth. Each example shows a transverse reconstruction and associated multi-label model outputs for the 3D sub-volume patch. Ground truth labels are listed in bold text, and predicted probabilities indicated by the gray bars. For example, Fig. 6b correctly predicts atelectasis + effusion with high probabilities for those two ground truth labels, and low probabilities for the other

three labels. l.stone= liver/gallbladder stone, l.lesion= liver/gallbladder lesion, k.stone= kidneys/ureters stone, k.lesion= kidneys/ureters lesion.

In general, classification of diffuse abnormalities was superior to focal abnormalities. For the lungs/pleura, AUC was  $> 0.8$  for the diffuse lung diseases of effusion and emphysema, moderate for atelectasis with AUC of 0.77, but poor for nodules with AUC of 0.65. For liver/gallbladder, fatty liver and dilation demonstrated the highest performance with AUC  $> 0.8$ , liver lesion was moderate at 0.73, while the stone class performed poorly with  $< 0.7$ . For the kidneys/ureters, performance was good at AUC  $> 0.80$  for kidney stone and atrophy classes, and moderate for kidney lesion (0.68) and cyst (0.70) classes. Examples of images that were classified shown in [Figure 6](#).

#### IV. DISCUSSION

The main purpose of this work was to create a weakly supervised 3D classification workflow that can be generalized to many diagnostic tasks in body CT. To test this workflow, we classified multiple diseases or normality among three different organ systems: lungs/pleura, liver/gallbladder, and kidneys/ureters. The organ systems and diseases were intentionally chosen to represent a wide variety of locations and appearances. Unlike conventional supervised learning, the proposed system used automated rules to analyze radiology text reports and avoid radiologist annotation efforts. This provides a form of weak supervision since each case-level label (e.g., lung nodule) applies to an entire organ, although the abnormality may be present in only a portion of the volume.

Our reported performances do not match that of traditional, fully supervised studies where individual findings are annotated. However, weak supervision offers several advantages. By using automated label extraction, we were able to label a vast data set from a large health system. Such a scalable approach allows better representation of diverse patient populations, scanner equipment/protocols, and organs/diseases. In contrast, manually curating and labeling such a large, diverse data set would be prohibitive.

Many of the existing studies in medical image AI have focused on a single abnormality or organ system (1, 4-6, 9, 25-27). To the best of our knowledge, we are one of the first to gather such a diverse dataset with 15 possible labels (12 abnormalities, and 3 normal labels for 3 different organ systems) from a large data set of over 13,000 body CT scans of over 12,000 unique subjects. Unlike common binary tasks such as disease presence vs. absence, performing

multi-label classification for several co-occurring diseases is exponentially more challenging. Furthermore, classification of multiple diseases/organs may have a different clinical application. Whereas a single disease model (e.g., lung nodule detection) targets radiologist performance for that disease, a broader approach that encompasses multiple diseases/organs may instead seek to improve workflow, such as to conduct computer-aided triage for cases with the highest or lowest likelihood of suspicion. Similar studies like Wang *et al.* (9) explored a multi disease classifier for 8 common thorax diseases in 2D chest radiography, and Draelos *et al.* (15) classified CTs with 83 abnormalities in the chest. While those studies were limited to the chest region, our study also extended this weak-supervision approach to other organs in the abdomen and pelvis. Our lung multi-class classification results are most comparable to the Draelos *et al.* (15) CT-Net-9 multi-label model trained with 9 abnormalities: nodule 0.65 vs. 0.68, atelectasis 0.77 vs 0.68, and pleural effusion 0.97 vs. 0.94 for our model versus CT-Net-9, respectively.

Compared to 2D CNN, working with 3D CNNs is computationally very expensive, especially for large CT volumes. For this reason, we downsampled the data to voxels of size  $2\text{ mm} \times 2\text{ mm} \times 2\text{ mm}$  to allow a reasonable balance between batch vs. patch sizes. This decreased resolution may account for the lower performance for focal disease like lung nodules, compared to diffuse disease like atelectasis and effusion. This trend was also observed for the liver/gallbladder and kidneys/ureters. Diffuse diseases such as fatty liver or renal atrophy performed well, while focal diseases such as gallstones and kidney lesions performed worse. There were a few notable exceptions, such as kidney stones that performed well with  $\text{AUC} > 0.8$ . This likely reflected the relative ease of detection because the CT scans for kidney cases tended to be from specialized kidney stone protocols.

This study has several limitations. This was a retrospective study from a single institution, and although the health system is composed of multiple hospitals, the patient population largely draws from a single geographic region, and reporting tendencies are likely to overlap amongst radiologists from the same department. Although this study encompassed multiple organs, the selected three sets of organ systems were independently processed for disease classification. This simplified the challenges that could be imposed by the interactions of multiple organs. Moreover, we considered only a few of the most common abnormalities, but results could have been confounded by co-occurrence of other diseases that were not otherwise analyzed. Finally, there were inevitable errors in our

rule-based labeling due to the complexity of sentences, diversity of expression in free-text narration, and typographical errors. Literature suggests that 2-20% of radiology text reports are estimated to contain demonstrable errors (28). However, studies have shown that such errors can be ameliorated with large amounts of data (29). Other studies have used natural language processing that may provide more accurate analysis of the report text (30-32).

Our future work will investigate important data extraction issues such as the relationship of CT resolution on classification performance, particularly stratified to the size of abnormalities. As a key step towards developing a universal abnormality detector, it will be necessary to understand the relationship between different, co-occurring abnormalities, including those with overlapping radiologic appearance such as pneumonia vs. atelectasis. Although study represented the typical case mix of a health system, it would also be useful to study the effect of class balance and performance. It will also be advantageous to augment the training data with less commonly encountered abnormalities and with variations in acquisition protocols, such as scans acquired without intravenous contrast material or with lower radiation doses. This will enrich the training and improve the generalization of the system. We also plan to make the CT reports and volumes used in this study publicly available pending deidentification and approval.

Overall, weak supervision offers a number of general advantages. By using automated label extraction, we were able to efficiently annotate a vast data set from a large health system, which in turn enabled the development of image classifiers for multiple organs and multiple diseases. Such a scalable approach is a step closer to satiating data-hungry deep learning models for medical imaging, where manually curating and labeling tens of thousands of cases would be prohibitive in terms of time and expense.

#### ACKNOWLEDGMENTS

We are grateful for helpful discussions with and data collection by Ricardo Henao PhD, Rachel Draelos, Songyue Han, Khrystyna Faryna, Vignesh Selvakumaran MD, James Tian MD, Mark Kelly MD, Ehsan Abadi PhD, and Brian Harrawood.

## REFERENCES

- Kim H-E, Kim HH, Han B-K, Kim KH, Han K, Nam H, Lee EH, Kim E-K. Changes in cancer detection and false-positive recall in mammography using artificial intelligence: a retrospective, multireader study. *The Lancet Digital Health* 2020;2(3):e138-e148. doi: 10.1016/s2589-7500(20)30003-0
- Esteve A, Kuprel B, Novoa RA, Ko J, Swetter SM, Blau HM, Thrun S. Dermatologist-level classification of skin cancer with deep neural networks. *Nature* 2017;542(7639):115-118. doi: 10.1038/nature21056
- Mori Y, Kudo SE, Misawa M, Saito Y, Ikematsu H, Hotta K, Ohtsuka K, Urushibara F, Kataoka S, Ogawa Y, Maeda Y, Takeda K, Nakamura H, Ichimasa K, Kudo T, Hayashi T, Wakamura K, Ishida F, Inoue H, Itoh H, Oda M, Mori K. Real-Time Use of Artificial Intelligence in Identification of Diminutive Polyps During Colonoscopy: A Prospective Study. *Ann Intern Med* 2018;169(6):357-366. doi: 10.7326/M18-0249
- Lin H, Li R, Liu Z, Chen J, Yang Y, Chen H, Lin Z, Lai W, Long E, Wu X, Lin D, Zhu Y, Chen C, Wu D, Yu T, Cao Q, Li X, Li J, Li W, Wang J, Yang M, Hu H, Zhang L, Yu Y, Chen X, Hu J, Zhu K, Jiang S, Huang Y, Tan G, Huang J, Lin X, Zhang X, Luo L, Liu Y, Liu X, Cheng B, Zheng D, Wu M, Chen W, Liu Y. Diagnostic Efficacy and Therapeutic Decision-making Capacity of an Artificial Intelligence Platform for Childhood Cataracts in Eye Clinics: A Multicentre Randomized Controlled Trial. *EClinicalMedicine* 2019;9:52-59. doi: 10.1016/j.eclinm.2019.03.001
- Ciampi F, Chung K, van Riel SJ, Setio AAA, Gerke PK, Jacobs C, Scholten ET, Schaefer-Prokop C, Wille MMW, Marchionò A, Pastorino U, Prokop M, van Ginneken B. Towards automatic pulmonary nodule management in lung cancer screening with deep learning. *Sci Rep* 2017;7:46479. doi: 10.1038/srep46479
- Ding Y, Sohn JH, Kawczynski MG, Trivedi H, Harnish R, Jenkins NW, Lituiev D, Copeland TP, Aboian MS, Mari Aparici C, Behr SC, Flavell RR, Huang SY, Zalocusky KA, Nardo L, Seo Y, Hawkins RA, Hernandez Pampaloni M, Hadley D, Franc BL. A Deep Learning Model to Predict a Diagnosis of Alzheimer Disease by Using (18)F-FDG PET of the Brain. *Radiology* 2019;290(2):456-464. doi: 10.1148/radiol.2018180958
- Willemink MJ. Preparing Medical Imaging Data for Machine Learning. *Radiology* 2020;295(1):4-15.
- Johnson AEW. MIMIC-CXR, a de-identified publicly available database of chest radiographs with free-text reports. *Sci Data* 2019;6(1):317.
- Wang X, Peng Y, Lu L, Lu Z, Bagheri M, Summers RM. ChestX-Ray8: Hospital-Scale Chest X-Ray Database and Benchmarks on Weakly-Supervised Classification and Localization of Common Thorax Diseases. 2017 IEEE Conference on Computer Vision and Pattern Recognition (CVPR)2017; p. 3462-3471.
- Irvin J, Rajpurkar P, Ko M, Yu Y, Ciurea-Ilcus S, Chute C, Marklund H, Haghighi B, Ball R, Shpanskaya K. Chexpert: A large chest radiograph dataset with uncertainty labels and expert comparison. *Proceedings of the AAAI Conference on Artificial Intelligence*2019; p. 590-597.
- Yan K, Wang X, Lu L, Summers RM. DeepLesion: automated mining of large-scale lesion annotations and universal lesion detection with deep learning. *J Med Imaging (Bellingham)* 2018;5(3):036501. doi: 10.1117/1.JMI.5.3.036501
- Yan K, Wang X, Lu L, Zhang L, Harrison AP, Bagheri M, Summers RM. Deep lesion graph in the wild: relationship learning and organization of significant radiology image findings in a diverse large-scale lesion database. In: Lu L, Wang X, Carneiro G, Yang L, eds. *Deep Learning and Convolutional Neural Networks for Medical Imaging and Clinical Informatics*. Cham: Springer International Publishing, 2019; p. 413-435.
- Yan K, Peng Y, Sandfort V, Bagheri M, Lu Z, Summers RM. Holistic and comprehensive annotation of clinically significant findings on diverse CT images: learning from radiology reports and label ontology. *IEEE Conference on Computer Vision and Pattern Recognition*. Long Beach, CA, USA2019.
- Yan K, Peng Y, Sandfort V, Bagheri M, Lu Z, Summers RM. Holistic and comprehensive annotation of clinically significant findings on diverse CT images: learning from radiology reports and label ontology. *Proceedings of the IEEE Conference on Computer Vision and Pattern Recognition*2019; p. 8523-8532.
- Draeos RL, Dov D, Mazurowski MA, Lo JY, Henao R, Rubin GD, Carin L. Machine-learning-based multiple abnormality prediction with large-scale chest computed tomography volumes. *Med Image Anal* 2021;67:101857. doi: 10.1016/j.media.2020.101857
- Eyuboglu S, Angus G, Patel BN, Pareek A, Davidzon G, Long J, Dunnmon J, Lungren MP. Multi-task weak supervision enables anatomically-resolved abnormality detection in whole-body FDG-PET/CT. *Nature Communications* 2021;12(1):1880. doi: 10.1038/s41467-021-22018-1
- Saha A, Tushar FI, Faryna K, D'Anniballe VM, Hou R, Mazurowski MA, Rubin GD, Lo JY, Hahn HK, Mazurowski MA. Weakly supervised 3D classification of chest CT using aggregated multi-resolution deep segmentation features. *Medical Imaging 2020: Computer-Aided Diagnosis*2020.
- Han S, Tian J, Kelly M, Selvakumaran V, Henao R, Rubin GD, Lo JY, Hahn HK, Mori K. Classifying abnormalities in computed tomography radiology reports with rule-based and natural language processing models. *Medical Imaging 2019: Computer-Aided Diagnosis*2019.
- Faryna K, Tushar FI, D'Anniballe VM, Hou R, Rubin GD, Lo JY, Hahn HK, Mazurowski MA. Attention-guided classification of abnormalities in semi-structured computed tomography reports. *Medical Imaging 2020: Computer-Aided Diagnosis*2020.
- D'Anniballe VM, Tushar FI, Faryna K, Han S, Mazurowski MA, Rubin GD, Lo JY. Multi-Label Annotation of Chest Abdomen Pelvis Computed Tomography Text Reports Using Deep Learning. 2021;arXiv:2102.02959. Accessed February 01, 2021.
- Gibson E, Giganti F, Hu Y, Bonmati E, Bandula S, Gurusamy K, Davidson B, Pereira SP, Clarkson MJ, Barratt DC. Automatic multi-organ segmentation on abdominal CT with dense v-networks. *IEEE Trans Med Imaging* 2018;37(8):1822-1834. doi: 10.1109/TMI.2018.2806309
- Segars PW. Population of anatomically variable 4D XCAT adult phantoms for imaging research and optimization. *Medical Physics* 2013;40(4):043701.
- He KM, Zhang XY, Sun J. Deep Residual Learning for Image Recognition. *Proc CVPR* 2019:770-778.
- Robin X, Turck N, Hainard A, Tiberti N, Lisacek F, Sanchez J-C, Müller M. pROC: an open-source package for R and S+ to analyze and compare ROC curves. *BMC Bioinformatics* 2011;12(1):77. doi: 10.1186/1471-2105-12-77
- Johnson AEW, Pollard TJ, Berkowitz SJ, Greenbaum NR, Lungren MP, Deng CY, Mark RG, Horng S. MIMIC-CXR, a de-identified publicly available database of chest radiographs with free-text reports. *Sci Data* 2019;6(1):317. doi: 10.1038/s41597-019-0322-0
- Schelh P, Kohl S, Radtke JP, Wiesenfarth M, Kickingereder P, Bickelhaupt S, Kuder TA, Stenzinger A, Hohenfellner M, Schlemmer HP, Maier-Hein KH, Bonekamp D. Classification of Cancer at Prostate MRI: Deep Learning versus Clinical PI-RADS Assessment. *Radiology* 2019;293(3):607-617. doi: 10.1148/radiol.2019190938
- Yala A, Schuster T, Miles R, Barzilay R, Lehman C. A Deep Learning Model to Triage Screening Mammograms: A Simulation Study. *Radiology* 2019;293(1):38-46. doi: 10.1148/radiol.2019182908
- Brady A, Laoide R, McCarthy P, McDermott R. Discrepancy and error in radiology: concepts, causes and consequences. *Ulster Med J* 2012;81(1):3-9.
- Mahajan D, Girshick R, Ramanathan V, He K, Paluri M, Li Y, Bharambe A, van der Maaten L. Exploring the limits of weakly supervised pretraining. *Proceedings of the European Conference on Computer Vision (ECCV)*2018; p. 181-196.
- Banerjee I, Ling Y, Chen MC, Hasan SA, Langlotz CP, Moradzadeh N, Chapman B, Amrhein T, Mong D, Rubin DL, Farri O, Lungren MP. Comparative effectiveness of convolutional neural network (CNN) and recurrent neural network (RNN) architectures for radiology text report classification. *Artif Intell Med* 2019;97:79-88. doi: 10.1016/j.artmed.2018.11.004
- Steinkamp JM, Chambers CM, Lalevic D, Zafar HM, Cook TS. Automated Organ-Level Classification of Free-Text Pathology Reports to Support a Radiology Follow-up Tracking Engine. *Radiology: Artificial Intelligence* 2019;1(5):e180052. doi: 10.1148/ryai.2019180052
- Shin H-C, Lu L, Summers RM. Natural Language Processing for Large-Scale Medical Image Analysis Using Deep Learning. *Deep Learning for Medical Image Analysis*2017; p. 405-421.



**Table 1:** Total number (#) of volumes associated with each label for lungs/pleura, liver/gallbladder, and kidneys/ureters (from left to right). Each volume may contain one or more organs and/or disease labels. Normal cases contain no abnormalities. A total of 19,255 labels from 13,667 volumes contributing to the data within this table, were from 12,092 unique subjects.

Lungs/Pleura		Liver/Gallbladder		Kidneys/Ureters	
Label	# volumes	Label	# volumes	Label	# volumes
Atelectasis	1,758	Stone	1,088	Stone	1,188
Nodule	1,628	Lesion	1,716	Lesion	1,685
Emphysema	1,194	Dilatation	628	Atrophy	683
Effusion	1,465	Fatty	1,108	Cyst	1,449
Normal	1,396	Normal	1,123	Normal	1,146

**Table 2:** RBA performance for 2,158 radiology reports across 15 labels using manually obtained ground truth.

Lungs/Pleura				Liver/Gallbladder				Kidneys/Ureters			
Label	# Pos	Acc	F-score	Label	# Pos	Acc	F-score	Label	# Pos	Acc	F-score
Atelectasis	251	0.98	0.97	Stone	144	0.96	0.91	Stone	174	0.93	0.85
Nodule	296	0.92	0.89	Lesion	224	0.95	0.92	Lesion	238	0.91	0.86
Emphysema	193	0.99	0.98	Dilation	87	0.98	0.92	Atrophy	94	0.99	0.97
Effusion	205	0.98	0.97	Fatty	166	0.98	0.96	Cyst	234	0.96	0.94
Normal	209	0.98	0.96	Normal	166	0.96	0.93	Normal	194	0.96	0.92

Note: # Pos= number of positive examples for that label in report test set, Acc=Accuracy.